International Journal of Heat and Mass Transfer 169 (2021) 120979

Contents lists available at ScienceDirect

International Journal of Heat and Mass Transfer

journal homepage: www.elsevier.com/locate/hmt

Effects of mass and interaction mismatches on in-plane and cross-plane thermal transport of Si-doped graphene

Yu-Kai Weng, Ali Yousefzadi Nobakht, Seungha Shin*, Kenneth D. Kihm, Douglas S. Aaron

Department of Mechanical, Aerospace, and Biomedical Engineering, The University of Tennessee, Knoxville, TN 37996, USA

ARTICLE INFO

Article history:
Received 16 September 2020
Revised 8 January 2021
Accepted 11 January 2021
Available online 22 January 2021

Keywords:
Thermal transport
Graphene
Si doping
Phonon scattering
Molecular dynamics

ABSTRACT

The effects of silicon (Si) doping on the in-plane and cross-plane thermal transport of suspended and silicon dioxide (SiO_2) supported graphene were investigated via molecular dynamics simulations. Due to the large mismatch in atomic mass and interaction with neighboring carbon atoms, Si can act as an effective phonon scatterer, thus suppressing the thermal transport. In this study, we evaluated the contributions of mass and interaction mismatches of Si dopants to the reduction in the in-plane thermal conductivity and the cross-plane thermal resistance through systematic control of the dopant's properties. 2% Si doping reduces the in-plane transport of suspended graphene by ~94% due to the increased scattering, while the SiO_2-supported graphene is less affected. The phonon scattering by Si linearly increases with the Si content, and the interaction mismatch has a greater influence on the phonon kinetics during in-plane transport than the mass mismatch. In contrast, the cross-plane transport is enhanced by Si doping, decreasing the interfacial thermal resistance by ~30%, because of the stronger interfacial interactions by weaker in-plane bonding and the smaller atomic mass mismatch with the substrate material. The enhanced understanding of doping effects on thermal transport from this research is expected to provide insights for effective thermal transport control in various graphene structures.

1. Introduction

Graphene, as the first example of a two-dimensional (2D) atomic crystal [1], has been a highly focused subject for scientific investigation because its 2D hexagonal carbon lattice structure provides unique electronic [2], mechanical [3], optical [4], and thermal [5,6] properties. These exceptional properties make graphene a promising material in various applications (e.g., graphene-based transistors, monolithically integrated circuits, optical modulators, and electromagnetic wave shields [7,8]). Specifically, the high thermal conductivity of graphene (4,800-5,300 W/m-K [9]) is desirable for thermal management applications requiring rapid heat transfers. On the other hand, high thermal conductivity is unfavorable for some applications, such as thermoelectric (TE) systems, which show promise for energy harvesting and recovery applications [10]. The TE performance is characterized by the figure-of-merit (ZT), which is inversely proportional to the thermal conductivity (k) of the TE material; ZT increases with the electrical conductivity (σ) and the Seebeck coefficient (S) [11] ($ZT = \sigma S^2 T/k$). Thus, to enhance the potential of graphene on thermoelectric applications, effective thermal transport control, while maintaining or enhancing the electrical and TE conversion properties (σ and S), is a critical task.

For the thermal transport control of graphene, several approaches have been introduced, including edge passivation [12], geometrical defects [13], isotope engineering [14], strain [15], and grain boundary [16,17]. In addition to these approaches, doping is another effective method to modify the thermal transport properties of graphene [18] and other semiconductor materials [19], because additional phonon scattering by impurities or dopants eventually leads to the thermal transport reduction. Since atomic mass and interaction mismatches affect impurity scattering, the doping-induced thermal transport reduction is dependent on the dopant's species. Several materials, such as nitrogen (N) [20], boron (B) [21], gold (Au), platinum (Pt), and nickel (Ni) [22], have been examined as possible elements to modify the properties of graphene. However, doping can also change or degrade other properties for TE or electronic performance (σ and S); thus, to minimize the influence on electrical properties, the doping of silicon (Si), which has an electronic structure similar to C, was suggested [18].

Si-doped graphene was successfully synthesized with controlled Si concentrations [23] and actively studied for mechanical and electrical properties [24]. Its thermal transport has been explored due to their application potentials for TE [18,25]; however, the detailed mechanism and effectiveness of the heat transfer suppres-

* Corresponding author.
E-mail address: sshin@utk.edu (S. Shin).

https://doi.org/10.1016/j.ijheatmasstransfer.2021.120979
0017-9310/

sion by Si doping are still unclear. Also, since other elements are often added to graphene structures by doping or functionalization, this research will be beneficial for the evaluation or control of thermal transport in various graphene applications, such as graphene electrodes [26]. Furthermore, supported graphene has not been addressed, even though graphene is usually supported by a dielectric substrate in the electronic devices [27], since it is not able to sustain the structure itself. Thermal transport of supported graphene has more complexities than that of the suspended graphene due to additional interfacial interactions [28] between the graphene and the substrate. Thus, in addition to in-plane thermal conductivity, the out-of-plane thermal transport, characterized by interfacial thermal resistance or conductance [29], also needs to be examined. Here, we selected crystalline silicon dioxide (SiO_2) as a substrate material due to its wide range of applications, such as photovoltaics, semiconductor electronic devices, catalysis, film substrates, ceramics, and humidity sensors [30,31]. Moreover, the use of SiO_2 crystal facilitates the analysis of the Si-doping effects, as structural disorder is excluded, different from amorphous SiO_2.

In this study, the in-plane and out-of-plane thermal transport of Si-doped graphene was investigated by using molecular dynamics (MD) simulations [32,33]. In the following sections, the subject structures, simulation procedure, and methodologies of thermal transport analysis are described in more detail. Then, we present the in-plane thermal conductivity of the suspended Si-doped graphene and its sensitivity to mass and interaction mismatch, followed by the discussion of the in-plane and out-of-plane thermal transport in SiO_2-supported Si-doped graphene systems. Through this research, we evaluate the effects of mass and interaction mismatches on the in-plane and out-of-plane thermal transport in Si-doped graphene and discuss the physical mechanisms of thermal transport changes through the phonon kinetics and phonon spectrum.

2. Methodology

In this research, MD simulations of suspended and SiO_2-supported Si-doped single-layer graphene were performed using Large-scale Atomic/Molecular Massively Parallel Simulator (LAMMPS) [34]. The interaction forces between C atoms within Si-doped graphene were calculated using the Tersoff-2010 potential model [35]. Tersoff-2010 reproduces various graphene phonon properties accurately and requires a reasonable level of computing cost [36]. Tersoff-type potential models were also used for Si-C systems within Si-doped graphene [37], and for Si-O systems within a SiO_2 substrate [38]. The interlayer interactions between an atom within Si-doped graphene (Si or C) and one in the SiO_2 substrate (Si or O) were calculated using the 12-6 Lennard-Jones (LJ) potential function with the parameters from the Universal-Force Field (UFF) [39]. The Verlet algorithm [40] was employed to integrate Newton's equations of motion within the simulation domain with a single time step of 0.5 fs. Several common verification techniques for MD data (e.g., validation of potential and kinetic energy convergence, and structural stability) were performed for all the simulations to ensure that the presented results were physically sound and scientifically meaningful. The nonequilibrium (NE) temperature setup was primarily used for the thermal transport analysis. However, MD simulations of the suspended graphene with an equilibrium (E) temperature setup were also conducted to confirm the thermal transport control by Si doping, excluding the effects of the simulation cell size (the two setups are denoted as NEMD and EMD, respectively).

The atomic configurations of the suspended and supported graphene are shown in Fig. 1a and b. A single layer of graphene is simulated, and x and y are defined as the in-plane directions. Si doping was implemented by randomly replacing C atoms with Si atoms in the graphene sheet while the dopant concentration varied from 0.0% to 2.0% with an increment of 0.2%. Although the examined concentrations are rather high when compared with conventional doping, Si or N dopants in graphene can readily reach the high doping levels in experiments [41–43]. In addition, this wide concentration range was selected to clearly observe the effects of doping concentration on the phonon kinetics and thermal transport.

The additional phonon scattering, which affects the phonon transport in Si-doped graphene, was attributed to the heavier atomic mass of Si and weaker C-Si interactions, in comparison to lighter C atoms and strong C-C interactions. To distinguish the effects of the mass and interaction mismatches, the following three setups for Si doping were employed: i) using the actual Si atomic mass (m_{Si} = 28.086 g/mole) while the C-C interaction model [37] was used for C-Si interatomic interactions (mass mismatch only); ii) using the C-Si interaction model [37] while using the same atomic mass as C for the doped Si atoms (interaction mismatch only); and iii) including both the mass and interaction mismatches (mass + interaction effect).

In NEMD, the temperature distribution and thermal transport were induced by non-equilibrium temperature settings [44,45]. All of the NEMD simulations in this research employed a graphene length (x-direction) of l = 50 nm and width (y-direction) of w = 20 nm. For in-plane thermal transport, hot and cold thermostats were applied to the two opposite ends of graphene in the x-direction. The boundary conditions are periodic in the y-direction and free boundary in the z- direction. To examine thermal transport at T, the temperatures of the hot and cold thermostats (T_H and T_C) were set as T + 25 K and T – 25 K. Initial equilibration was performed for 0.5 ns in the *NVT* ensemble (constant number of particles, volume, and temperature) by re-scaling velocities to a prescribed temperature. After the equilibration was completed, five layers of carbon atoms (≈ 0.45 nm) were fixed at both ends of the structure to prevent heat leakage to the periodic mirror of the sample at the ends. Hot and cold Langevin thermostats were then applied near these fixed regions for 14 layers of carbon atoms (≈ 1.4 nm) to generate a heat flux within the simulation sample [12,45]. Atomic data for the thermal transport analysis were collected from 2.0 ns of additional simulations after the equilibration.

In NEMD, the heat flux, $\boldsymbol{q}$ (W/m^2), between the hot and cold thermostats was determined by calculating the amounts of energy transfer in/out through the thermostats per unit time and unit cross-section area. The heat flux can also be calculated using the ensemble average of heat flux vector $\boldsymbol{q}_f$, i.e., $\boldsymbol{q} = \langle \boldsymbol{q}_f \rangle$, given as:

$$q_f = \frac{1}{V}\left[\sum_i \frac{1}{2} m_i (u_i \cdot u_i) u_i + \sum_i \varphi_i u_{i,x} + \frac{1}{2}\sum_i \sum_j r_{ij}(u_i \cdot F_{ij})\right], \quad (1)$$

where V is the volume; m_i, $\boldsymbol{u_i}$, and φ_i are the mass, velocity vector, and potential energy of atom i, respectively; and $\boldsymbol{r_{ij}}$ and $\boldsymbol{F}_{ij}$ are the position and interaction force vectors between i and j particles. The spacing of the graphene sheet was selected as the thickness of the single-layer graphene (t = 0.335 nm) for the cross-sectional area ($A_c = wt$). For the temperature gradient ∇T (= dT/dx in 1D), the temperature distribution was estimated from the average of the local kinetic energies. Using Fourier's law, i.e., $\boldsymbol{q} = -k\nabla T$, the in-plane thermal conductivity k (W/m-K) was calculated.

The in-plane thermal conductivity of suspended Si-doped graphene was also calculated using an equilibrium temperature setup. In the EMD simulations, the length and width of the graphene sheet were 15.0 nm and 5.0 nm, respectively. The initial equilibration was performed under the *NPT* ensemble (constant number of particles, pressure, and temperature) with velocity rescaling for 2 ns. Then, switching to *NVE* (constant number of particles, volume, and energy), it was continued for 13 ns, and the

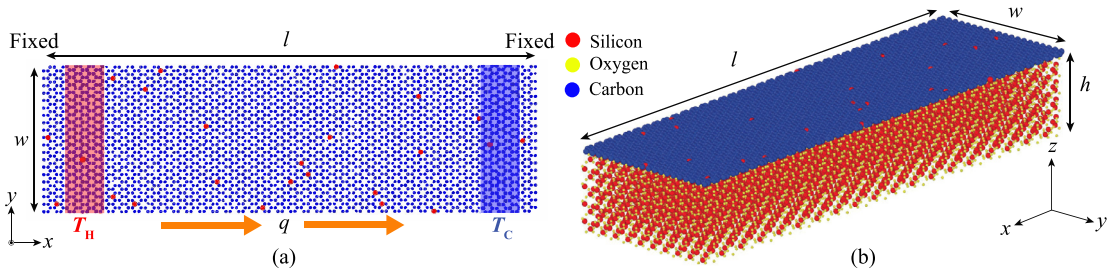

Fig. 1. Configurations of simulation cells for (a) suspended and (b) SiO_2 supported Si-doped graphene.

resulting data were recorded during the last 5 ns. Once the data recording was finished, the thermal conductivity was calculated by the Green-Kubo method, which takes a time integral of the heat flux auto-correlation function (HACF), as follows:

$$k = \frac{1}{Vk_BT^2}\int_0^\infty \langle q_f(0)q_f(t)\rangle dt, \tag{2}$$

where k_B is the Boltzmann constant, and angular brackets ($\langle\ \rangle$) are used for the ensemble average.

For the in-plane thermal transport of the supported graphene with a SiO_2 substrate (Fig. 1b), the graphene and the SiO_2 substrate had the same length and width dimensions as the suspended graphene of the NEMD simulations, and the height of the SiO_2 substrate (h) was 3.28 nm. Hot and cold thermostats were applied to both the graphene and substrate, which ensured the same temperature distribution and minimized the heat transfer between the two materials. As in the suspended cases, the in-plane thermal conductivity of the supported graphene was examined using the T-distribution and the average heat flux on graphene [29].

In addition to in-plane thermal conductivity, the cross-plane thermal transport across the graphene/SiO_2 interface was also investigated by employing the temperature relaxation method [46,47]. The graphene/SiO_2 system was first equilibrated at 300 K; then, hot and cold thermostats at 350 K and 250 K were placed on the graphene and SiO_2 substrate, respectively. After reaching a steady state, the thermostats were removed to initiate the thermal relaxation of the simulated structure. During the relaxation period, the temperatures and energy changes of graphene and SiO_2 substrate were recorded. The interfacial thermal resistance, R (m^2-K/W), was then obtained by [46]:

$$R = \frac{\int_0^t A(T_{\text{graphene}} - T_{SiO_2})dt}{E_t - E_0}, \tag{3}$$

where E_t is the total energy of the supported graphene; E_0 is the initial energy of graphene at the beginning of the relaxation period; A is the area of graphene/SiO_2 interface; and T_{graphene} and T_{SiO2} are the temperatures of graphene and SiO_2, respectively.

To understand the detailed mechanisms of the thermal transport change by Si doping, we examined the changes in atomic structure and phonon properties. Specifically, the bond length difference near Si dopants from the C-C bonding was examined by calculating the distribution of interatomic distances [$\rho_{N,i\text{-}j}(r)$] [48], which describes the distribution of the number density of atomic distance r between atom species i and j, given as:

$$\rho_{N,i-j}(r) = \lim_{dr\to 0}\frac{N_{i-j}(r)}{4\pi r^2\left(N_{tot,i-j}/V\right)dr}, \tag{4}$$

where $N_{i\text{-}j}(r)$ is the average number of i-j atom pairs found at a distance between r and $r + dr$; $N_{tot,i\text{-}j}$ is the total number of the atom pairs in the system; and V is the total volume of the system.

Among phonon properties, the phonon density of states (D_p) and lifetime (τ_p) were examined to characterize their spectrum and kinetics. D_p was calculated by the Fourier transform of velocity-autocorrelation function [49]. For the D_p calculation, velocity data of over 100 sampled atoms were collected at every time step (0.5 fs) for 25 ps in equilibrium MD simulations at 300 K. Phonon lifetime calculations employed the lattice dynamics and normal mode decomposition [33,50,51], and using the normalized autocorrelation of total energy (E, including kinetic and potential energy), the lifetime (τ_p) of a phonon with wavevector κ and mode ν was calculated as:

$$\frac{\langle E(\kappa_\nu;t)E(\kappa_\nu;0)\rangle}{\langle E(\kappa_\nu;0)E(\kappa_\nu;0)\rangle} = \exp(-t/\tau_p). \tag{5}$$

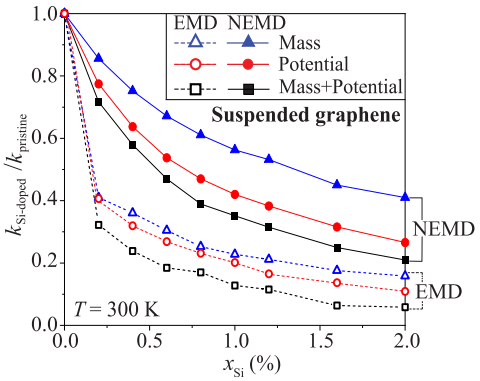

Fig. 2. The reduction of in-plane thermal transport of Si-doped graphene compared with pristine graphene ($k_{\text{Si-doped}}/k_{\text{pristine}}$) with respect to the Si content (x_{Si}). The reduction is more significant in the EMD simulations (dashed lines with the empty symbols) than the NEMD (solid lines with the filled symbols). Inclusion of mass (blue triangles) or interaction (red circles) mismatch only leads to a smaller thermal transport reduction than in the cases with both mismatches by Si dopants (black squares), and the interaction mismatch is more effective in reducing thermal transport than the mass mismatch. (For interpretation of the references to color in this figure legend, the reader is referred to the web version of this article.).

3. Results and discussion

Effective reduction of the in-plane thermal transport of suspended graphene by Si-doping was observed in MD simulations. Specifically, in NEMD simulations, 79.0% of reduction was achieved with 2% of Si content (Fig. 2). The reduction of thermal transport is characterized as the ratio of the thermal conductivity of Si-doped graphene ($k_{\text{Si-doped}}$) and that of the pristine graphene (k_{pristine}), i.e., $k_{\text{Si-doped}}/k_{\text{pristine}}$. $k_{\text{Si-doped}}/k_{\text{pristine}}$ decreases as the Si concentration increases, and the decrease becomes slower as the Si content increases. Excluding the mass or interaction mismatch effect results in a smaller reduction, and the mismatch between Si-C and C-C interaction strengths is more effective for the reduction of thermal conduction than the mass mismatch between Si and C.

Similar behaviors of thermal conductivity reduction are observed in the EMD simulations as in Fig. 2. However, the reduction in EMD (94.2% at $x_{\text{Si}} = 2\%$) is more significant than that in NEMD, especially when the Si content is small. Since the majority of atomic masses and interactions are unchanged among the

simulated systems, the phonon dispersion remains almost invariant, and so do the phonon energy and group velocity. Thus, the phonon transport control by Si doping can be attributed mainly to the changes in the phonon kinetics. In the MD simulations here, phonon could be scattered by other phonons, boundaries, impurities (Si), substrate, etc. Then, according to Matthiessen's rule [52], the overall phonon scattering rate ($\dot{\gamma}_p$) or the inverse of phonon lifetime ($1/\tau_p$) is expressed as:

$$\dot{\gamma}_p(=1/\tau_p) = \dot{\gamma}_{p-p} + \dot{\gamma}_{p-im} + \dot{\gamma}_{p-sub} + \dot{\gamma}_{p-others}, \quad (6)$$

where $\dot{\gamma}_{p-p}$, $\dot{\gamma}_{p-im}$, and $\dot{\gamma}_{p-sub}$ are the phonon scattering rates by interaction with other phonons, impurities, and the substrate, respectively, and $\dot{\gamma}_{p-others}$ represents the phonon interaction with other effects (e.g. thermostat, system boundary, etc.) in the MD simulations of this research. Here, the effects of coupling between different scattering mechanisms were excluded, considering each Si dopant as an isolated impurity scatterer. If included, a larger increase in the overall scattering rate (i.e. more reduction in heat transfer) may be induced by higher doping concentrations [53].

Here, we control $\dot{\gamma}_{p-im}$ by Si doping, and the phonon-impurity scattering strength (Γ, where $\dot{\gamma}_{p-im} \propto \Gamma$) is affected by mass and interaction mismatch as given by [54]:

$$\Gamma = \sum_i f_i \left[\left(1 - \frac{M_i}{\bar{M}}\right)^2 + \varepsilon\gamma^2 \left(1 - \frac{R_i}{\bar{R}}\right)^2 \right], \quad (7)$$

where f_i is the fractional concentration of the foreign atoms, and γ and ε are the Grüneisen and phenomenological parameters, respectively. M_i and R_i are the mass and the radius of the i-th substitutional atom. $\bar{M}$ and $\bar{R}$ represent average atomic mass and radius, which are the same as for pristine graphene (i.e. $\bar{M} = M_C$ and $\bar{R} = R_{C\text{-}C}$). A larger concentration of dopant would enlarge f_i, which would increase phonon scattering by impurities, reducing the thermal conductivity. As demonstrated in Eq. (7), more phonon scattering can be induced by a larger mass mismatch [larger $(\bar{M} - M_i)/\bar{M}$] or larger bond strength difference [larger $(\bar{R} - R_i)/\bar{R}$]. Using the atomic masses of Si and C ($M_{Si} = M_i = 28.086$ g/mole and $M_C = \bar{M} = 12.011$ g/mole), the mass difference is readily calculated. We estimated the mismatch in the interaction term in Eq. (7) by comparing the force constant matrix of a single C atom in pristine graphene and that of a doped Si atom (surrounded by C atoms), both of which were calculated from the Hessian matrix ($\boldsymbol{H}$, i.e., the second-order derivatives) of the potential energy. The element of the Hessian matrix for the interaction between coordinate a of atom i and b of j is given as $H_{ij,ab} = \partial^2 E/\partial r_{i,a}\partial r_{j,b}$, where $r_{i,a}$ and $r_{j,b}$ are the atomic positions of i and j in a and b coordinates, respectively. Comparison of the L2-norms of the Hessian matrices from C-C and Si-C interactions shows that the interaction between the Si-C is considerably lower than the interaction between C-C ($||\boldsymbol{H}_{Si\text{-}C}||/||\boldsymbol{H}_{C\text{-}C}|| \approx 0.04$). This large interaction mismatch results in the bond length difference ($R_{C\text{-}C} = 1.47$ Å and $R_{C\text{-}Si} = 1.77$ Å), as the distributions of Si-C and C-C interatomic distance [$r_{N,Si\text{-}C}(r)$ and $r_{N,C\text{-}C}(r)$] in Fig. 3a demonstrates. Using the mass and bond length mismatch induced by Si doping ($|(\bar{M} - M_i)/\bar{M}| \approx 1.33$ and $|(\bar{R}\bar{R} - R_i)/\bar{R}| \approx 0.22$), we approximated the scattering rate of phonon-Si interaction with a proportionality constant C as:

$$\dot{\gamma}_{p-Si} = C x_{Si}\left(1.33^2 + \varepsilon\gamma^2 0.22^2\right). \quad (8)$$

Then, the scatterings from the mass mismatch effect only and from a potential mismatch only ($\dot{\gamma}_{p-Si}|_{mass}$ and $\dot{\gamma}_{p-Si}|_{potential}$, respectively) can be expressed as $1.33^2 C x_{Si}$ and $0.22^2 C x_{Si}\varepsilon\gamma^2$, respectively.

Thermal conductivity is inversely proportional to the phonon scattering rate ($\dot{\gamma}_p$) according to the kinetic theory, and additional scattering $\dot{\gamma}_{p-Si}$ is added to the pristine graphene scattering ($\dot{\gamma}_{p,pristine}$) with Si doping ($\dot{\gamma}_{p,Si-doped} = \dot{\gamma}_{p,pristine} + \dot{\gamma}_{p-Si}$). Thus, the reduction of in-plane thermal transport of Si-doped graphene can be expressed as:

$$\frac{k_{Si-doped}}{k_{pristine}} = \frac{\dot{\gamma}_{p,pristine}}{\dot{\gamma}_{p,pristine} + \dot{\gamma}_{p-Si}} = \frac{1}{1 + \dot{\gamma}_{p-Si}/\dot{\gamma}_{p,pristine}}. \quad (9)$$

Using $k_{Si\text{-}doped}/k_{pristine}$ from MD and Eq. (9), $\dot{\gamma}_{p-Si}/\dot{\gamma}_{p,pristine}$ with respect to x_{Si} is estimated (Fig. 3b), and in all the simulated cases, the linear increase of scattering with x_{Si} is observed. Fitting the $\dot{\gamma}_{p-Si}/\dot{\gamma}_{p,pristine}$ from NEMD to Eq. (8), C_{NE} ($=C/\dot{\gamma}_{p,pristine,NEMD}$) and $\varepsilon\gamma^2$ were calculated as 52.12 and 50.13, respectively. The scattering rates using the fitted parameters agree well with those from MD for all three cases of Si doping consideration, which supports the validity of Eq. (8) and the fitting parameters. On the other hand, $\dot{\gamma}_{p-Si}/\dot{\gamma}_{p,pristine}$ from EMD leads to a larger C_E ($= C/\dot{\gamma}_{p,pristine,EMD} =$ 168.2) using the same $\varepsilon\gamma^2$, and this is attributed to a lower phonon scattering rate in EMD than NEMD, as it can exclude additional scattering from a nonequilibrium thermostat setup. The larger C_E and $\dot{\gamma}_{p-Si}/\dot{\gamma}_{p,pristine}$ explain the larger reduction in k, especially at low x_{Si}.

The above analysis using Eq. (9) is based on the single-relaxation time approximation that does not address the spectral dependence of phonon scattering. As Fig. 3c shows, the relaxation time τ_p from the lattice dynamics calculations with the normal-mode decomposition [50] decreases with increasing phonon energy (E_p), i.e., more phonon scattering at high E_p. However, the changes in the calculated τ_p by Si doping agree with the k calculations; that is, the Si-C potential mismatch leads to shorter τ_p than the mass mismatch, resulting in lower k, and the inclusion of both mass and potential mismatches is the most effective factor in enhancing phonon scattering, reducing τ_p and k.

In Si-doped graphene supported by SiO_2, the interaction between the SiO_2 substrate and Si-doped graphene imposes additional scattering by the substrate ($\dot{\gamma}_{p-sub}$). In particular, the substrate interaction affects the scattering of out-of-plane phonons, which are the primary thermal energy carriers in suspended graphene; thus, in-plane thermal transport is largely reduced by adding a substrate [55]. Due to this additional $\dot{\gamma}_{p-sub}$, the relative contribution of $\dot{\gamma}_{p-Si}$(or $\dot{\gamma}_{p-im}$) to overall phonon scattering ($\dot{\gamma}_p$) [Eq. (6)] in the supported Si-doped graphene becomes smaller than in the suspended cases. Therefore, although thermal conductivity (k) reduction and their mass and potential mismatch effects on k reduction are observed similarly to the suspended Si-doped graphene, suppressing the in-plane thermal transport by Si doping is less effective, as shown in Fig. 4a. As in the suspended cases, using the k reduction ($k_{Si\text{-}doped}/k_{pristine}$) in Fig. 4a and Eq. (9), we calculated the scattering strength of phonon-Si dopant interaction in supported Si-doped graphene ($\dot{\gamma}_{p-Si}/\dot{\gamma}_{p,pristine}$) compared with overall phonon scattering in the supported pristine graphene (Fig. 4b). For all three Si doping considerations (mass, potential, and mass + potential), $\dot{\gamma}_{p-Si}/\dot{\gamma}_{p,pristine}$ increases linearly with x_{Si} and has a good fit to a Si scattering model based on Eq. (8), using $C_{Supported}$ ($= C/\dot{\gamma}_{p,pristine,Supported}$) of 32.47 and the same $\varepsilon\gamma^2$ in the suspended cases. Here, the smaller $C_{Supported}$ by a larger $\dot{\gamma}_{p,pristine,Supported}$ supports the smaller reduction in k by Si doping.

Interfacial thermal transport between Si-doped graphene and SiO_2 substrate was examined by analyzing the interfacial temperature difference ($\Delta T_{graphene/SiO2}$) and energy of graphene ($E_{graphene}$) during thermal relaxation. As shown in Fig 5a, graphene and SiO_2 substrate almost reach a thermal equilibrium within 150 ps, and the linear relation between $E_{graphene}$ and the time integral of $\Delta T_{graphene/SiO2}$ is observed during the relaxation period. Using the linear relation with Eq. (3), the interfacial thermal resistance $R_{graphene/SiO2}$ was calculated for various doping cases. As presented in Fig. 5b, while Si doping reduces in-plane thermal transport in graphene, interfacial thermal transport between the graphene and SiO_2 substrate is enhanced by Si doping, i.e., $R_{graphene/SiO2}$ decreases

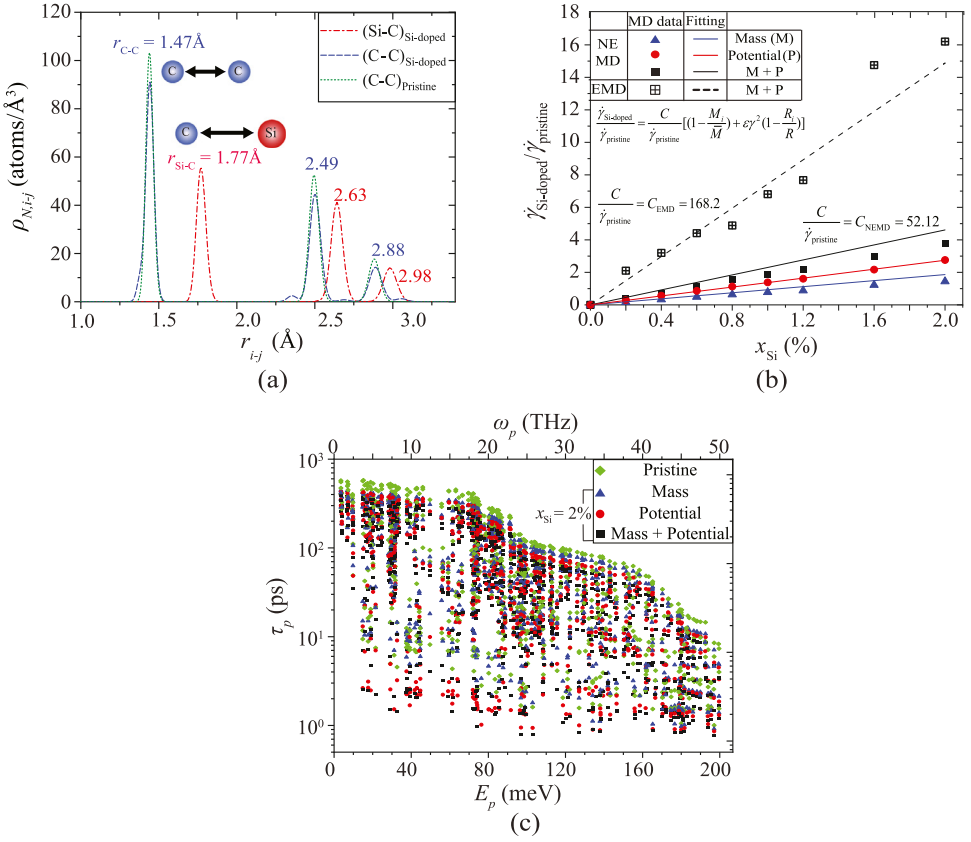

Fig. 3. (a) Distributions of Si-C (red) and C-C interatomic distance (blue and green) [$\rho_{N,\text{Si-C}}(r)$ and $\rho_{N,\text{C-C}}(r)$] in suspended pristine and Si-doped graphene, showing that Si increases the bond length. (b) Scattering strength of phonon-Si interaction compared with the pristine graphene from NEMD (filled) and EMD simulations (dashed) and Eq. (9). The lines represent models with fitting parameters using Eq. (8). (c) Phonon lifetime (τ_p) of pristine graphene (green diamonds) and 2% Si-doped graphene with respect to phonon energy (E_p) and frequency (ω_p). In both (b) and (c), Si doping includes mass mismatch only (blue triangles), potential mismatch only (red circles), and both mismatches (black squares). (For interpretation of the references to color in this figure legend, the reader is referred to the web version of this article.).

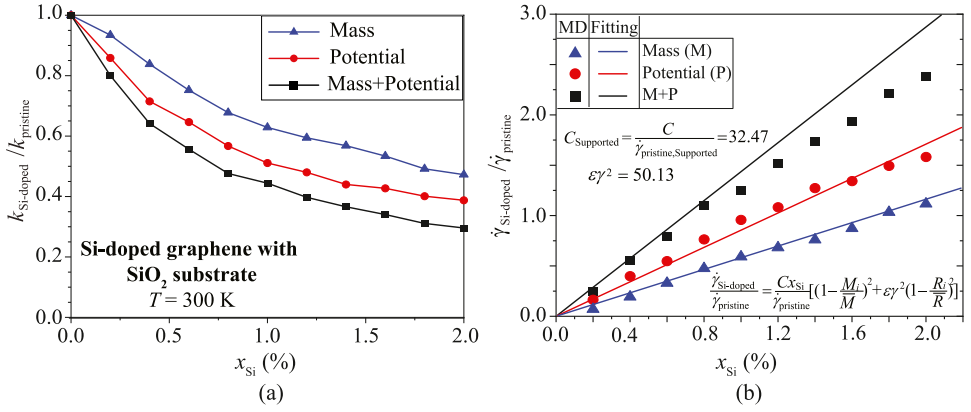

Fig. 4. (a) The reduction of in-plane thermal transport of SiO_2 supported Si-doped graphene compared with pristine graphene ($k_{\text{Si-doped}}/k_{\text{pristine}}$) with respect to the Si content (x_{Si}). (b) Scattering strength of phonon-Si interaction in supported Si-doped graphene, including mass mismatch only (blue triangles), potential mismatch only (red circles), and both mismatches (black squares), compared with the supported pristine graphene. The lines represent models with fitting parameters using Eq. (8). (For interpretation of the references to color in this figure legend, the reader is referred to the web version of this article.).

with increasing x_{Si}. It is also observed that the inclusion of a potential mismatch in Si doping leads to a larger enhancement in cross-plane thermal transport than the cases including the Si-C mass mismatch only.

The weakened intralayer bonding by Si doping allows for a larger displacement of doped Si atoms in the z direction, which leads to a smaller distance between substrate and Si dopants, as shown in Fig. 5c. The smaller interlayer distance does not appear when including the mass mismatch only, demonstrating that the distance difference originates from the weak Si-C bonding. The interlayer interaction between Si-doped graphene and SiO_2 substrate is stronger with a shorter atomic distance [29], therefore yielding a larger thermal transport or lower interlayer thermal resistance. This interfacial transport enhancement by Si doping can be regarded as the phonon focusing effect [56], which explains the negative correlation between in-plane and cross-plane thermal transport. Although the Si doping with mass mismatch only does not intensify the interlayer interaction strength, the heavier mass of

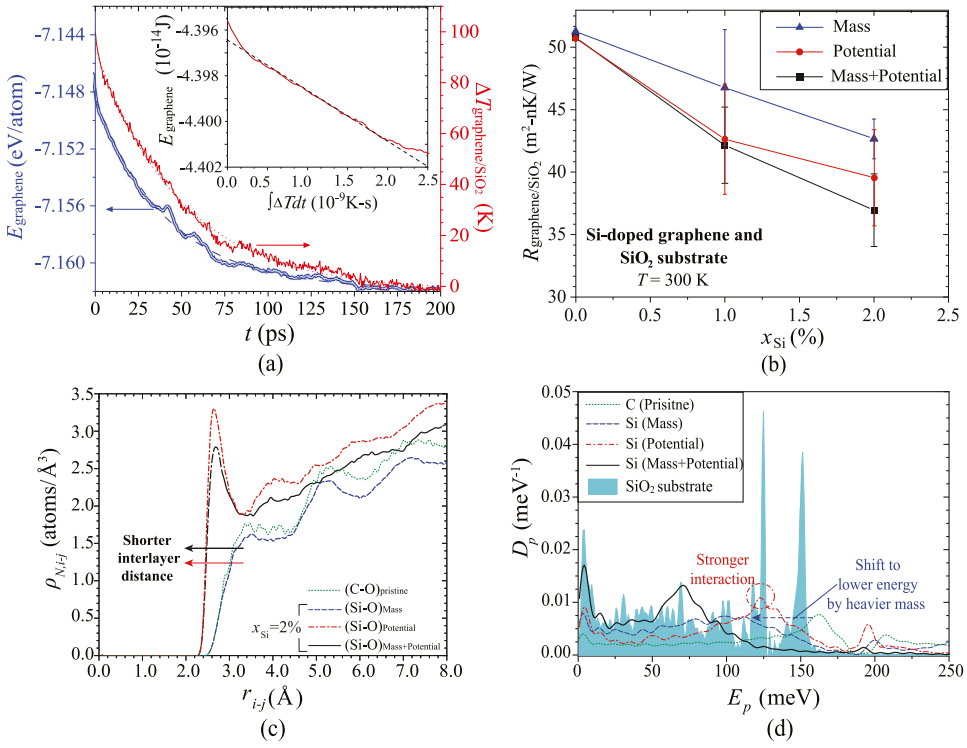

Fig. 5. (a) Evolution of interfacial T difference ($\Delta T_{\text{graphene/SiO2}}$) and graphene energy ($E_{\text{graphene}}$) during thermal relaxation and linear relation between E_{graphene} and the time integral of $\Delta T_{\text{graphene/SiO2}}$ (inset). (b) Interfacial thermal resistances ($R_{\text{graphene/SiO2}}$) between Si-doped graphene ($x_{\text{Si}} = 0$, 1%, and 2%) and SiO_2 substrate with error bars (standard deviation of five simulation results). (c) Distributions of interatomic distance between O atoms in the substrate and Si dopants in the Si-doped graphene or C atoms in the pristine graphene [$\rho_{N,\text{Si-O}}(r)$ and $\rho_{N,\text{C-O}}(r)$], showing that Si doping with the potential mismatch reduces the interlayer atomic distance. (d) Phonon density of state (D_p) of C atoms in pristine graphene (green, dashed) and Si dopants in 2% Si-doped graphene with mass mismatch only (blue), potential mismatch only (red), and both mismatches (black). The cyan shade represents D_p of the SiO_2 substrate near the interface (< 5 Å from the graphene) for comparison. (For interpretation of the references to color in this figure legend, the reader is referred to the web version of this article.).

Si dopants, which is more similar to SiO_2, lowers their vibration frequency, resulting in more resonant vibration than C atoms, as the phonon density of state (D_p) displays in Fig. 5d. Thus, D_p of Si dopants has a larger overlap with that of the SiO_2 substate than that of pristine graphene, which contributes to the interfacial thermal transport [49]. A large overlap in D_p is also observed in the case of Si doping with the potential mismatch, due to the stronger interlayer interactions. Combining the effects of heavier atomic mass and stronger interaction, Si doping effectively enhances the interlayer thermal transport.

4. Conclusions

The effects of Si doping on thermal transport in graphene were examined using molecular dynamics simulations under various conditions, and the physical mechanisms of the resulting thermal transport changes were identified based on the analysis of atomic structural and vibrational properties and phonon kinetics. The added Si atoms have a larger atomic mass and weaker interatomic interaction than their neighboring C atoms. Due to the weak in-plane atomic bonds, the Si-C bond length is longer than C-C, and Si dopants have a shorter interlayer distance with the SiO_2 substrate. The mass mismatch and the structural change by interaction (potential) mismatch enhance the phonon scattering during in-plane transport. According to our MD simulations, the additional scattering is proportional to x_{Si}, and the interaction mismatch contributes more to the scattering enhancement than the mass mismatch. The increase in the phonon scattering reduces the in-plane thermal transport, and the reduction is more significant when the Si-phonon scattering dominates over the other scattering mechanisms; thus, the thermal conductivity of the suspended graphene decreases more drastically by the Si doping (reduced by ~94% with $x_{\text{Si}} = 2\%$) than the supported graphene case. In contrast, Si doping increases the interfacial transport between graphene and substrate (by ~30% with $x_{\text{Si}} = 2\%$) because the atomic vibration of Si is more resonant with the SiO_2 substrate due to their atomic mass similarity, and the shorter interlayer distance by the weak in-plane bonding strengthens the interlayer interactions. As in the in-plane transport, the effect of interaction mismatch on the interfacial transport is larger than that of Si atomic mass mismatch.

Physical understanding of the Si doping effects on graphene thermal transport from this research provides insights on the control and evaluation of thermal transport properties in various graphene heterostructures, including other elements. Effective control and accurate evaluation of thermal transport will benefit not only the development of thermoelectric devices, but also in other graphene applications, such as graphene electrodes. In a future study, more diverse functional groups and doping elements can be employed for an enhanced thermal system design and analysis of diverse graphene devices, and the modal analysis of phonon kinetics in doped graphene will be beneficial for a more in-depth physical understanding.

Declaration of Competing Interest

The authors declare that they have no known competing financial interests or personal relationships that could have appeared to influence the work reported in this paper.

CRediT authorship contribution statement

Yu-Kai Weng: Methodology, Software, Validation, Formal analysis, Investigation, Data curation, Writing - original draft, Visualization. **Ali Yousefzadi Nobakht:** Methodology, Investigation, Data

curation, Writing - original draft. **Seungha Shin:** Conceptualization, Methodology, Writing - original draft, Writing - review & editing, Supervision. **Kenneth D. Kihm:** Conceptualization, Writing - review & editing. **Douglas S. Aaron:** Conceptualization, Writing - review & editing.

Acknowledgment

The authors gratefully acknowledge the financial support by the U.S. National Science Foundation (Grant No. CBET-1933800). This work utilized the resources of Extreme Science and Engineering Discovery Environment (XSEDE), which is supported by National Science Foundation Grant number ACI-1053575. Y.-K Weng and A. Yousefzadi Nobakht appreciate fruitful discussions with Jiaqi Wang, Md Abdullah Al Hasan, and Junhyun Sung.

References

[1] K.S. Novoselov, Nobel lecture: graphene: materials in the flatland, Rev. Mod. Phys. 83 (3) (2011) 837–849.
[2] K. Nomura, A.H. MacDonald, Quantum transport of massless Dirac fermions, Phys. Rev. Lett. 98 (7) (2007) 076602.
[3] I.W. Frank, D.M. Tanenbaum, A.M. van der Zande, P.L. McEuen, Mechanical properties of suspended graphene sheets, J. Vac. Sci. Technol. B 25 (6) (2007) 2558–2561.
[4] L.A. Falkovsky, Optical properties of graphene, J. Phys. Conf. Ser. 129 (2008) 012004.
[5] K.M.F. Shahil, A.A. Balandin, Thermal properties of graphene and multilayer graphene: applications in thermal interface materials, Solid State Commun. 152 (15) (2012) 1331–1340.
[6] D.C. Marable, S. Shin, A. Yousefzadi Nobakht, Investigation into the microscopic mechanisms influencing convective heat transfer of water flow in graphene nanochannels, Int. J. Heat Mass Transf. 109 (2017) 28–39.
[7] X. Du, I. Skachko, A. Barker, E.Y. Andrei, Suspended graphene: a bridge to the Dirac point, Nat. Nanotechnol. 3 (2008) 491–495.
[8] P. Avouris, F. Xia, Graphene applications in electronics and photonics, MRS Bull. 37 (12) (2012) 1225–1234.
[9] A.A. Balandin, S. Ghosh, W. Bao, I. Calizo, D. Teweldebrhan, F. Miao, C.N. Lau, Superior thermal conductivity of single-layer graphene, Nano Lett. 8 (3) (2008) 902–907.
[10] D. Dragoman, M. Dragoman, Giant thermoelectric effect in graphene, Appl. Phys. Lett. 91 (20) (2007) 203116.
[11] R. Verma, S. Bhattacharya, S. Mahapatra, Thermoelectric performance of a single-layer graphene sheet for energy harvesting, IEEE Trans. Electron Devices 60 (6) (2013) 2064–2070.
[12] J. Hu, S. Schiffli, A. Vallabhaneni, X. Ruan, Y.P. Chen, Tuning the thermal conductivity of graphene nanoribbons by edge passivation and isotope engineering: A molecular dynamics study, Appl. Phys. Lett. 97 (13) (2010) 133107.
[13] A. Yousefzadi Nobakht, S. Shin, K.D. Kihm, D.C. Marable, W. Lee, Heat flow diversion in supported graphene nanomesh, Carbon 123 (2017) 45–53.
[14] S. Chen, Q. Wu, C. Mishra, J. Kang, H. Zhang, K. Cho, W. Cai, A.A. Balandin, R.S. Ruoff, Thermal conductivity of isotopically modified graphene, Nat. Mater. 11 (3) (2012) 203–207.
[15] N. Wei, L. Xu, H.-Q. Wang, J.-C. Zheng, Strain engineering of thermal conductivity in graphene sheets and nanoribbons: a demonstration of magic flexibility, Nanotechnology 22 (10) (2011) 105705.
[16] A.Y. Serov, Z.-Y. Ong, E. Pop, Effect of grain boundaries on thermal transport in graphene, Appl. Phys. Lett. 102 (3) (2013) 033104.
[17] W. Lee, K.D. Kihm, H.G. Kim, S. Shin, C. Lee, J.S. Park, S. Cheon, O.M. Kwon, G. Lim, W. Lee, In-plane thermal conductivity of polycrystalline chemical vapor deposition graphene with controlled grain sizes, Nano Lett. 17 (4) (2017) 2361–2366.
[18] W. Lee, K.D. Kihm, H.G. Kim, W. Lee, S. Cheon, S. Yeom, G. Lim, K.R. Pyun, S.H. Ko, S. Shin, Two orders of magnitude suppression of graphene's thermal conductivity by heavy dopants (Si), Carbon 138 (2018) 98–107.
[19] M.I. Baraton, Functionalization of semiconductor nanoparticles, in: Functionalized Nanoscale Materials, Devices and Systems, Springer, 2008, pp. 77–86.
[20] T. Zhang, J. Li, Y. Cao, L. Zhu, G. Chen, Tailoring thermal transport properties of graphene by nitrogen doping, J. Nanopart. Res. 19 (2) (2017) 48.
[21] T.B. Martins, R.H.d. Miwa, A.J.R. Da Silva, A. Fazzio, Electronic and transport properties of boron-doped graphene nanoribbons, Phys. Rev. Lett. 98 (19) (2007) 196803.
[22] Y. Gan, L. Sun, F. Banhart, One-and two-dimensional diffusion of metal atoms in graphene, Small 4 (5) (2008) 587–591.
[23] R. Lv, M.C. Dos Santos, C. Antonelli, S. Feng, K. Fujisawa, A. Berkdemir, R. Cruz-Silva, A.L. Elías, N. Perea-Lopez, F. López-Urías, Large-area Si-doped graphene: controllable synthesis and enhanced molecular sensing, Adv. Mater. 26 (45) (2014) 7593–7599.
[24] M.S.S. Azadeh, A. Kokabi, M. Hosseini, M. Fardmanesh, Tunable bandgap opening in the proposed structure of silicon-doped graphene, Micro Nano Lett. 6 (8) (2011) 582–585.
[25] B.S. Lee, J.S. Lee, Thermal conductivity reduction in graphene with silicon impurity, Appl. Phys. A 121 (3) (2015) 1193–1202.
[26] S.-J. Kwon, T.-H. Han, T.Y. Ko, N. Li, Y. Kim, D.J. Kim, S.-H. Bae, Y. Yang, B.H. Hong, K.S. Kim, S. Ryu, T.-W. Lee, Extremely stable graphene electrodes doped with macromolecular acid, Nat. Commun. 9 (1) (2018) 2037.
[27] T. Das, B.K. Sharma, A.K. Katiyar, J.-H. Ahn, Graphene-based flexible and wearable electronics, J. Semicond. 39 (1) (2018) 011007.
[28] J.H. Seol, I. Jo, A.L. Moore, L. Lindsay, Z.H. Aitken, M.T. Pettes, X. Li, Z. Yao, R. Huang, D. Broido, Two-dimensional phonon transport in supported graphene, Science 328 (5975) (2010) 213–216.
[29] A. Yousefzadi Nobakht, S. Shin, Anisotropic control of thermal transport in graphene/Si heterostructures, J. Appl. Phys. 120 (22) (2016) 225111.
[30] R.N. Puspitasari, H.A. Budiarti, A.M. Hatta, S. Koentjoro, D.D. Risanti, Enhanced dye-sensitized solar cells performance through novel core-shell structure of gold nanoparticles and nano-silica extracted from Lapindo Mud Vulcano, Proc. Eng. 170 (2017) 93–100.
[31] M. Sadeghi, M. Dorodian, M. Rezaei, Synthesis and characteristic of precipitated nano-silica, J. Adv. Chem. 6 (1) (2013) 917–922.
[32] W.J. Evans, L. Hu, P. Keblinski, Thermal conductivity of graphene ribbons from equilibrium molecular dynamics: effect of ribbon width, edge roughness, and hydrogen termination, Appl. Phys. Lett. 96 (20) (2010) 203112.
[33] M. Vohra, A. Yousefzadi Nobakht, S. Shin, S. Mahadevan, Uncertainty quantification in non-equilibrium molecular dynamics simulations of thermal transport, Int. J. Heat Mass Transf. 127 (2018) 297–307.
[34] S. Plimpton, Fast parallel algorithms for short-range molecular dynamics, J. Comput. Phys. 117 (1) (1995) 1–19.
[35] L. Lindsay, D.A. Broido, Optimized Tersoff and Brenner empirical potential parameters for lattice dynamics and phonon thermal transport in carbon nanotubes and graphene, Phys. Rev. B 81 (20) (2010) 205441.
[36] M. Marcel, J. Maultzsch, E. Dobardžić, S. Reich, I. Milosevic, M. Damnjanovic, A. Bosak, C.M. Kirsch, C. Thomsen, Phonon dispersion of graphite by inelastic X-ray scattering, Phys. Rev. B 76 (3) (2007) 035439.
[37] J. Tersoff, Modeling solid-state chemistry: interatomic potentials for multicomponent systems, Phys. Rev. B 39 (8) (1989) 5566–5568.
[38] S. Munetoh, T. Motooka, K. Moriguchi, A. Shintani, Interatomic potential for Si–O systems using Tersoff parameterization, Comput. Mater. Sci. 39 (2) (2007) 334–339.
[39] A.K. Rappe, C.J. Casewit, K.S. Colwell, W.A. Goddard, W.M. Skiff, UFF, a full periodic table force field for molecular mechanics and molecular dynamics simulations, J. Am. Chem. Soc. 114 (25) (1992) 10024–10035.
[40] L. Verlet, Computer "experiments" on classical fluids. I. Thermodynamical properties of Lennard-Jones molecules, Phys. Rev. 159 (1) (1967) 98–103.
[41] Z. Wang, P. Li, Y. Chen, J. Liu, W. Zhang, Z. Guo, M. Dong, Y. Lia, Synthesis, characterization and electrical properties of silicon-doped graphene films, J. Mater. Chem. C 3 (2015) 6301–6306.
[42] R. Lv, M. Cristina dos Santos, C. Antonelli, S. Feng, K. Fujisawa, A. Berkdemir, R. Cruz-Silva, A. Elías, N. Perea-Lopez, F. López-Urías, H. Terrones, M. Terrones, Large-area si-doped graphene: controllable synthesis and enhanced molecular sensing, Adv. Mater. 26 (45) (2014) 7593–7599.
[43] D. Wei, Y. Liu, Y. Wang, H. Zhang, L. Huang, and G. Yu, "Synthesis of N-doped graphene by chemical vapor deposition and its electrical properties" *Nano Lett.*,2009. 9(5): pp. 1752-1758
[44] Z. Huang, Z. Tang, Evaluation of momentum conservation influence in non-equilibrium molecular dynamics methods to compute thermal conductivity, Phys. B 373 (2) (2006) 291–296.
[45] P.K. Schelling, S.R. Phillpot, P. Keblinski, Comparison of atomic-level simulation methods for computing thermal conductivity, Phys. Rev. B 65 (14) (2002) 144306.
[46] C.F. Carlborg, J. Shiomi, S. Maruyama, Thermal boundary resistance between single-walled carbon nanotubes and surrounding matrices, Phys. Rev. B 78 (20) (2008) 205406.
[47] B. Liu, J.A. Baimova, C.D. Reddy, A.W.-K. Law, S.V. Dmitriev, H. Wu, K. Zhou, Interfacial thermal conductance of a silicene/graphene bilayer heterostructure and the effect of hydrogenation, ACS Appl. Mater. Interfaces 6 (20) (2014) 18180–18188.
[48] M.A.A. Hasan, J. Wang, Y.C. Lim, A. Hu, S. Shin, Concentration dependence of hydrogen diffusion in α-iron from atomistic perspectives, Int. J. Hydrog. Energy 44 (51) (2019) 27876–27884.
[49] S. Shin, M. Kaviany, T. Desai, R. Bonner, Roles of atomic restructuring in interfacial phonon transport, Phys. Rev. B 82 (8) (2010) 081302.
[50] A.J.H. McGaughey, J.M. Larkin, Predicting phonon properties from equilibrium molecular dynamics simulations, Annu. Rev. Heat Transf. 17 (2014) 49–87.
[51] J.M. Larkin, J.E. Turney, A.D. Massicotte, C.H. Amon, A.J.H. McGaughey, Comparison and evaluation of spectral energy methods for predicting phonon properties, J. Comput. Theor. Nanosci. 11 (1) (2014) 249–256.
[52] M. Kaviany, Heat Transfer Physics, 2nd ed., Cambridge University Press, Cambridge, 2014.
[53] T. Feng, B. Qiu, X. Ruan, Coupling between phonon-phonon and phonon-impurity scattering: a critical revisit of the spectral matthiessen's rule, Phys. Rev. B 92 (23) (2015) 235206.
[54] P.G. Klemens, Theory of the a-plane thermal conductivity of graphite, J. Wide Bandgap Mater. 7 (4) (2000) 332–339.
[55] A. Vassighi, M. Sachdev, Thermal and Power Management of Integrated Circuits, Springer Publishing Company, Incorporated, 2010.
[56] Z. Wei, Y. Chen, C. Dames, Negative correlation between in-plane bonding strength and cross-plane thermal conductivity in a model layered material, Appl. Phys. Lett. 102 (1) (2013) 011901.